Open access • Journal Article • DOI:10.1007/S12289-016-1294-7

The bias-extension test for the analysis of in-plane shear properties of textile composite reinforcements and prepregs: a review — Source link

Philippe Boisse, Nahiene Hamila, E. Guzman-Maldonado, Angela Madeo ...+2 more authors

Institutions: University of Lyon, University of Orléans, Sapienza University of Rome

Published on: 01 Aug 2017 - International Journal of Material Forming (Springer Paris)

Topics: Slippage

The bias-extension test for the analysis of in-plane shear properties of textile composite reinforcements and prepregs: a review

P. Boisse, N. Hamila, E. Guzman-Maldonado, Angela Madeo, G. Hivet, F. Dell'Isola

The bias-extension test for the analysis of in-plane shear properties of textile composite reinforcements and prepregs: a review

P. Boisse[1] · N. Hamila[1] · E. Guzman-Maldonado[1] · A. Madeo[2] · G. Hivet[3] · F. dell'Isola[4]

Abstract The bias-extension test is a rather simple experiment aiming to determine in-plane shear properties of textile composite reinforcements. However the mechanics during the test involves fibrous material at large shear strains and large rotations of the fibres. Several aspects are still being studied and are not yet modeled in a consensual manner. The standard analysis of the test is based on two assumptions: inextensibility of the fibers and rotations at the yarn crossovers without slippage. They lead to the development of zones with constant fibre orientations proper to the bias-extension test. Beyond the analysis of the test within these basic assumptions, the paper presents studies that have been carried out on the lack of verification of these hypothesis (slippage, tension in the yarns, effects of fibre bending). The effects of temperature, mesoscopic modeling and tension locking are also considered in the case of the bias-extension test.

Keywords Bias extension · In-plane shear · Textile composite reinforcements · Prepregs

✉ P. Boisse
philippe.boisse@insa-lyon.fr

1 Université de Lyon, LaMCoS, INSA-Lyon, F-69621 Villeurbanne, France

2 Université de Lyon, LGCIE, INSA-Lyon, F-69621 Villeurbanne, France

3 Université d'Orléans, PRISME, F-45072 Orléans, France

4 Università di Roma "La Sapienza", DISG, Rome, Italy

Introduction

Textile composite reinforcements are usually made of yarns themselves composed of thousands of fibers, the diameter of which is very small (7 μm for a carbon fibre). The link of two initially orthogonal sets of yarns (warp and weft) allows to obtain a textile that can be seen as a quasi-continuous material. Warp and weft yarns can be woven following a 2D pattern (plain weave, twill or satin). In NCF (Non Crimp Fabrics) two layers (or more) of parallel yarns are linked by stitches in order to both insure coherence of the reinforcement and avoid crimp of the yarns. The interlock and 3D weavings link serval warp and weft yarn layers to obtain a large thickness. When the reinforcements are made of two yarn directions and when these yarns are linked by weaving or stitching, they can be shaped on a double curve surface. The fibres used in composites are quasi inextensible, consequently this shaping is obtained by in-plane shear of the textile reinforcement. For instance Fig. 1 shows the in-plane shear in the case of a hemispherical forming. Shaping (or draping) of prepregs is broadly similar. The resin present in the preimpregneted reinforcements is soft enough to render the forming by in-plane shear possible. In thermoset prepregs the resin is soft because it is not yet polymerized. Thermoplastic prepregs are heated over matrix melting temperature before forming. In all these cases in-plane shear of the textile reinforcement is the main deformation mode to obtain double curved shapes. For a given reinforcement they is a limit to shear angle. Over this value, wrinkling will appear (Fig. 2) [2–5]. This limit, often called 'locking angle', depends on textile reinforcement properties although there is no direct relation between shear angle and wrinkling. Wrinkling is a global phenomenon depending on all strains and stiffnesses and on boundary conditions [5].

Because in-plane shear is the main deformation mode of textile reinforcement during forming, it is the most studied

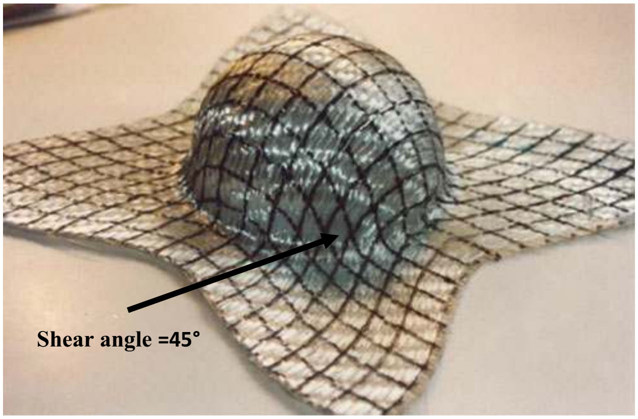

Fig. 1 Forming a woven reinforcement on a double curve shape requires in-plane shear deformations

property of textile composite reinforcement. It is an important data for draping simulations [6–10]. In LCM processes, the shear angle in the preform after draping modifies the permeability [11–14].

Studies on experimental fabric in-plane shear behavior started in the sixty's in particular with the works of Lindberg [15] and Grosberg [16, 17]. The physical phenomena during in-plane shear, such as contact and friction between the yarns are related to shearing properties. Spivak introduced in 1968 the 'test of bias-extension' as a relatively simple test that can be compared to 'rather sophisticated instrumental or experimental methods' that have been previously used to analyze in-plane shear properties [18]. Nevertheless the geometry and the resulting kinematics of the test are not yet specified. Skelton determines the limit shear angle from the geometry of the fabric and of the yarns [19]. McGuinness and O. Bradaigh experimentally analyses the shearing of fabric reinforced thermoplastic sheets using a picture frame test [20]. This picture frame test is one of the two main experiments used to measure textile reinforcement properties. The bias-extension test is the second one. The description of the bias-extension test with it specificities, the geometry of the specimen and the different shear zone was made by Wang et al. in 1998 [21]. The authors completed this work especially in term of prediction of the

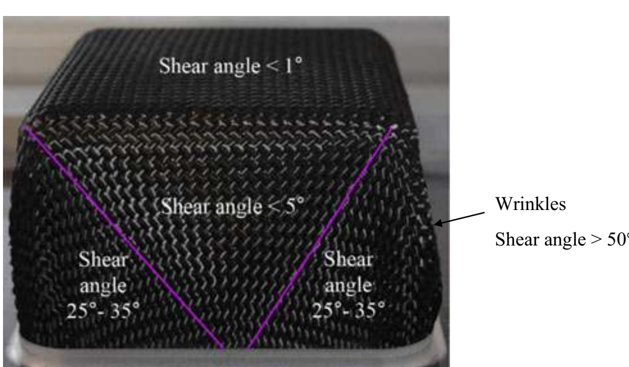

Fig. 2 Wrinkling induced by large shear angles [1]

shear force and analysis of yarn slippage [22, 23]. The bias-extension test is used to measure the in-plane shear characteristic of cross-plied unidirectional prepregs in [24].

The bias-extension test highlights several specific aspects due to the fibrous constitution of the specimen associated to large strains. The works on this shear test are numerous and some of them are recent. The objective of this paper is to make a survey of the works concerning the bias-extension test for textile composite reinforcements. First, based on basic assumptions, equations are given i.e. the relation between the in-plane shear angle and the specimen extension and the relation between the in-plane shear stress and the load on the tensile machine. This is not a simple point because the 'shear stress' is not defined in a consensual manner. Extension of the bias-extension test to high temperature tests that are necessary to analyze thermoplastic prepreg will be presented. Then, because the bias-extension test is based on strong assumptions, many studies concern their lack of verification. In particular, the influence of tension and of slippage in the specimen have been studied. The numerical simulation of the bias-extension test highlight difficulties especially, tension locking. The basic assumption assume constant in-plane shear zones and consequently a sharp transition of the fibre orientation at the change of zone. Actually transition areas exist between the zones that are due to fibre bending stiffness. These transition areas in the textile reinforcement can be modelled using macroscopic continuum models by introducing energies depending on second gradient of displacement. Finally the slippage in the bias-extension test will be analyzed by mesoscopic F.E. analyses i.e. modeling each yarn in contact and friction with its neighbors.

The two experimental tests to analyze in-plane shear properties of composite reinforcements

The picture-frame (trellis-frame) test (Fig. 3) and the bias-extension test (Fig. 4) are the two experimental tests mainly used for in-plane shear characterization of composite reinforcements and prepregs [25]. Some other tests have been proposed in which a rectangular fabric specimen is clamped on two opposite edges that prescribe an in-plane shear deformation to the specimen [15, 17, 26]. In these tests the specimen is generally subjected to shear and tensions. To avoid tensions, rigid bar can be added to the two free edges. In this case the test is close to picture frame. A shear test by means of torsion have been recently proposed for the analysis of UD prepregs (limited to small shear strains). Their mechanical behavior are specific because of the lack of cohesion in the direction normal to the fibres [27].

A picture frame, shown in Fig. 3 is a hinged frame with four rigid bars with equal length. A tensile force is applied across diagonally opposing corners of the picture frame rig

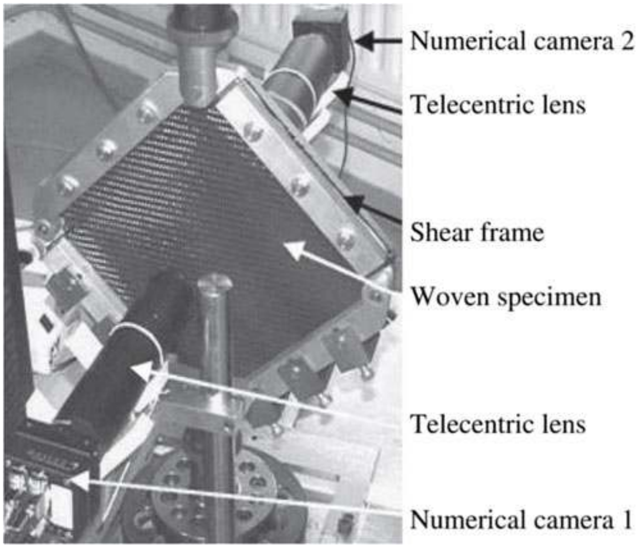

Fig. 3 Picture frame equipped with an optical system

causing the picture frame to move from an initially square geometry into a lozenge. The specimen within the picture frame is theoretically subjected to a pure and constant in-plane shear strain [2, 20, 25, 28, 29].

The bias-extension test consists in a tensile test on a rectangular textile reinforcement such that the warp and weft tow directions are orientated initially at 45° to the direction of the applied tension (Fig. 4). The initial length of the specimen must be more than twice the width of the specimen in a bias test. Under this condition, yarns in the central zone C are free at their both ends. If there is no slip between warp and weft yarn and assuming yarns being inextensible, the deformation in zone C is trellising and zone C is in pure shear. The shear angle in zones B is half those of zone C. One end of both warp and weft yarns of zone A is fixed in the clamp, consequently, assuming yarns being inextensible and no slip occurs, zone A remains undeformed. Finally, assuming the yarns do not extend, that there is no slip and neglecting the bending stiffness of the yarns, the bias-extension test leads to zones with constant in-plane shear (C), half in-plane shear (B) and undeformed (A). It is assumed that the in-plane shear is constant in each zone and this is first verified experimentally on bias-extension tests. Nevertheless it will be shown below that this assumption can be discussed.

The deformed shape with three zones, A,B,C is less simple that those of the picture frame where all the specimen is assumed to be subjected to a constant in-plane shear. Nevertheless a strong advantage of the bias-extension test lies in the fact that the yarns of the sheared zones are free at their edge (at least one) and consequently there is no tension in the yarns (or only small tensions due to the warp-weft interactions). In the picture frame all the yarns are clamped in the frame and any misalignment of the specimen will lead to an

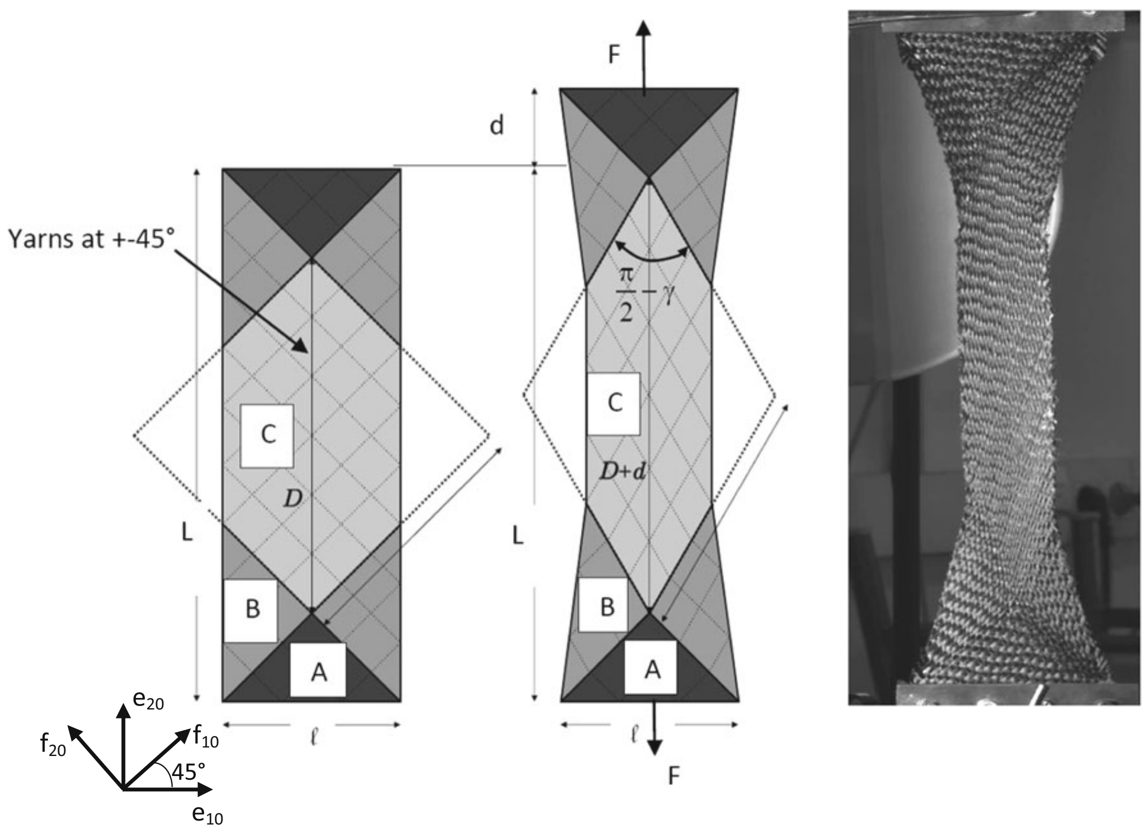

Fig. 4 Bias-extension test

increase of the measured load. Several comparison studies have be performed [30–33]. Figure 5 shows the shear force obtained with both experiments on a carbon woven fabric [33]. The picture frame result is much larger than the shear force measured by the picture frame. The picture frame used in this study allows to measure the tensions in the yarns and to adjust it to a given value. When this tension is set to zero, the result given by the picture frame is close to those of the bias-extension test. Measuring the in-plane shear in a textile material is difficult because the in-plane shear stiffness is small in comparison to tensile stiffness. Consequently any spurious tension during a test strongly perturbs the in-plane shear analysis. One main advantage of the bias-extension test lies in the absence of spurious tensions in the yarns of the sheared zones. Another advantage is its relative simplicity and its moderated size. This is important when the test is performed at high temperature in an oven. An in-plane shear benchmark has been realized by an international group of academic and industrial researchers on different composite reinforcements using both picture frame and bias-extension tests [25]. This benchmark has proved valuable for the community of composite materials because the materials and the tests are very different regarding continuous materials such as polymers or metals. It has been shown that the determination of the shear angle from the crosshead displacement is correct until 30–35°. Beyond this value, the direct measurement of the shear angle by optical methods is necessary. Finally the benchmark has shown that standardization methods are useful to obtain shear properties that can be used in numerical simulations.

Kinematics of the bias-extension test

Two relations are necessary to analyze the results of an in-plane shear test. A kinematic relation that relates the in-plane shear angle to the extension of the specimen and a relation between the shear stress in the fabric and the measured force on the tensile machine. To establish these relations, the following assumptions are made:

- yarns are inextensible (more precisely, their elongation is null in the bias-extension test),
- there is no slippage between warp and weft yarns at the cross over points,
- bending stiffness of yarn is neglected.

These three first assumptions correspond to those of the “kinematical models” or ‘fishnet algorithm’ used for fabric draping simulations based on geometry [34–36]. Consequently, the shear angles in the three zone A,B,C are constant in each zone.

The two relations of the bias-extension tests (kinematic relation and shear load versus force on the tensile machine) have been established gradually [25, 31, 33]. The first one is the relation between the shear angle γ in the central zone C and the length of the stretched specimen (given by the displacement of the tensile machine d) (Fig. 4):

$$\gamma = \frac{\pi}{2} - 2\text{Arccos}\left(\frac{D+d}{\sqrt{2}D}\right) \tag{1}$$

$D = L - \ell$ (Fig. 4) is the length of the central zone C. The shear angle γ can also be measured directly by an optical measure. Figure 6 shows the shear angle field obtained using a DIC measure (digital image correlation) [25, 37, 38]. This optical method is well suited for measurements of textile materials for which sensors in contact with the fabric are difficult to use. Optical analyses of the strain field at mesoscopic scale i.e. within the yarn have been done for in-plane shear test (Fig. 7) [37, 39]. The displacement field within the yarn is obtained by a DIC analysis at different stages of the shear test. For small angles the relative displacement field inside a yarn is a rotation field. Strains in the yarn are negligible. The shear load is mainly due to friction between the warp and weft

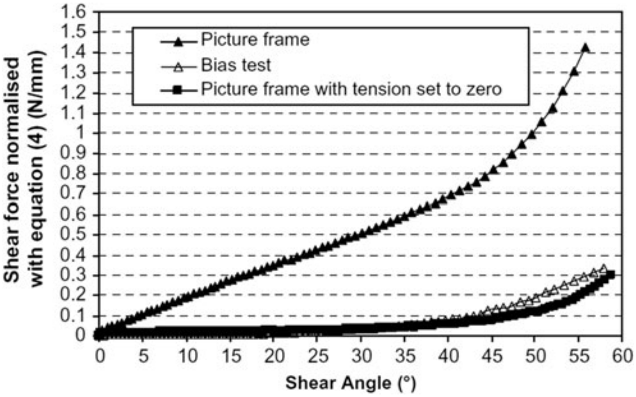

Fig. 5 Comparison of the shear force measured by a picture-frame and a bias-extension test [33]

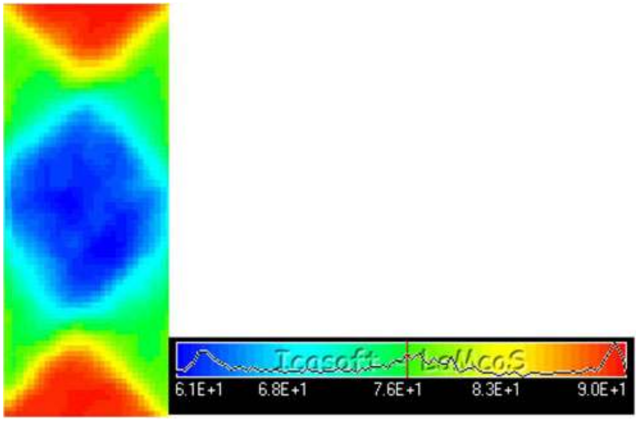

Fig 6 Shear angle in a plain weave fabric bias-extension test obtained from DIC [25]. (The angles given on the scales are 90°- γ)

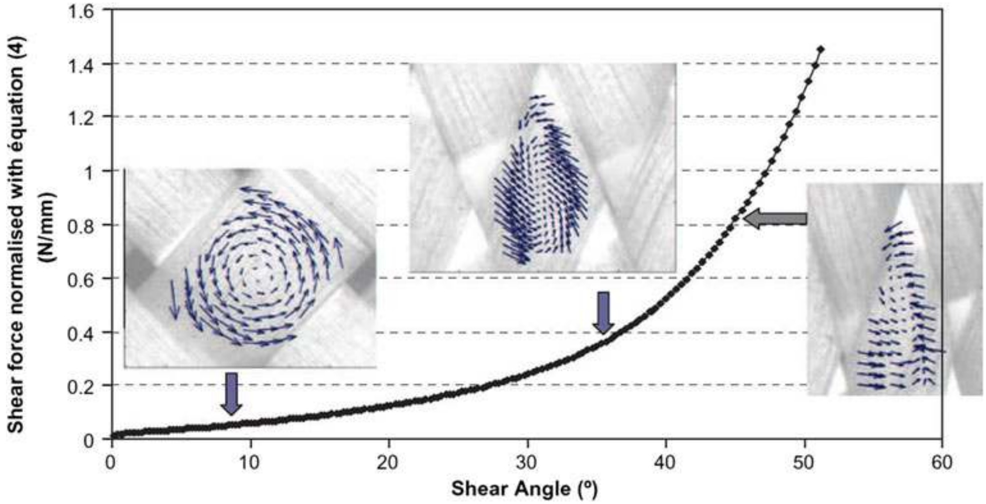

Fig. 7 Displacement field within a yarn at different stage of shearing

yarns. Then the geometry of the woven cell leads to yarns lateral contacts. The yarn is transversely compacted and this compaction is more important as the shear increases. It can lead to off-plane wrinkling.

Determination of shear forces

The shear angle is well accepted as the significant kinematic quantity in an in-plane shear test. The change of angle between warp and weft directions is simple and meaningful. There is no such simple and consensual quantity to characterize the efforts in the material during an in-plane shear test. In a bias-extension test the load on the tensile machine is measured. But it is a global quantity on the specimen. In order to compare the in-plane shear property obtained with different specimens or different devices and especially to use the in-plane shear properties in a model, this global load is not sufficient. It is necessary at least to transform this global load to a quantity that account for the geometry of the specimen. The vocabulary used in many articles by authors to achieve this, is 'normalisation'. That means obtain, from the load on the specimen, a load quantity independent of the geometry of the test and consequently that can be compared to other tests. Many papers have been written on this subject even recently [25, 32, 40–42]. The question is not simple. In a tensile test, the tensile stress can be obtained simply from the tensile load and the section of the specimen. For a shear test at small strains the shear stress can be calculated in the initial orthogonal Cartesian frame. It is not the case for in-plane shear test on textile reinforcement for which the shear angles are large. The directions of the warp and weft yarns rotate much and they must be followed to express the shear loads or shear stresses. In addition, if the comparison of two different tests is a justified goal, to model forming processes, it could also be interesting to have a 'load' quantity that is conjugated to the shear angle to obtain a power or a strain energy.

Shear load calculation

The shear load F_{sh} has been introduced in [25, 32, 33, 40, 43]. It is defined as the tangential load along the side of a fabric rhomboid element with unit dimensions (Fig. 8). These shear load create on the fabric element a torque (or moment) M_s :

$$M_s(\gamma) = F_{sh} \cos\gamma \tag{2}$$

$\gamma = \pi/2 - \alpha$ is the shear angle. α is the angle between the two warp and weft directions (Fig. 8).

It is possible to relate the shear load F_{sh} to the load on the machine F of the bias-extension test. Denoting S_B and S_C the initial areas of zone B and C [25, 33]:

$$F\dot{d} = M_s(\gamma)\ S_C\dot{\gamma} + M_s\left(\frac{\gamma}{2}\right)S_B\frac{\dot{\gamma}}{2} \tag{3}$$

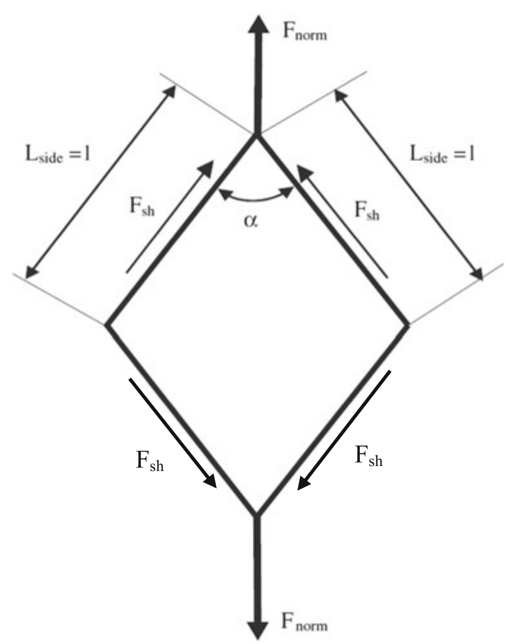

Fig. 8 Normalized load and shear load on a rhomboid with unit side

$M_s(\gamma)\ S_C\dot{\gamma}$ is the power of shear in the central part C of the specimen and $M_s\left(\frac{\gamma}{2}\right)S_B\frac{\dot{\gamma}}{2}$ is the power of shear in the zones B.

From the geometry of the specimen this leads to:

$$M_s(\gamma) = \frac{F\ D}{\ell(2D-\ell)}\left(\cos\frac{\gamma}{2} - \sin\frac{\gamma}{2}\right) - \frac{\ell}{2D-\ell}M_s\left(\frac{\gamma}{2}\right) \quad (4)$$

Using equation 2,

$$F_{sh}(\gamma) = \frac{F\ D}{\ell(2D-\ell)\cos\gamma}\left(\cos\frac{\gamma}{2} - \sin\frac{\gamma}{2}\right) - \frac{\ell\cos^{\gamma}/_2}{(2D-\ell)\cos\gamma}F_{sh}\left(\frac{\gamma}{2}\right) \quad (5)$$

Equation 5 gives $F_{sh}(\gamma)$ incrementally.

Shear moment calculation

The shear load, as defined above, permits to compare the bias-extension tests performed by different groups using different specimen geometries. It also permits to compare these results with picture frame tests [25]. Nevertheless it is not a quantity that is conjugated to the shear angle γ.

On the other hand, it is the case of the moment per surface M_s defined in equation 2. The loads on a woven unit cell (Fig. 9a) lead to the resultant tensions T_1, T_2, to the resultant bending moment M_1, M_2 and to the in-plane shear moment M_s. In a virtual displacement field η, the virtual in-plane shear work is

$$W_s(\eta) = \gamma(\eta)M_s \quad (6)$$

The shear moment M_s is a stress resultant. It is a result given by a bias extension on the specimen since it is related to the global load by equation (4). This in-plane shear virtual work (equation (6)) can be used in particular for the formulation of finite elements made of textile material [7, 39, 44, 45]. It can be notice that equation (5) that relates the shear load to the load on the machine, has been established using the shear moment M_s because it appears in the power balance (Equation 3).

Static approach

The relation between the shear moment and the load on the machine (4) can also be obtained from a static equilibrium. In Fig. 10, the case $L=2\ell$ is considered. The bias-extension test can be modeled as a hinged frame, the bars of which are submitted to a shear moment $M_{12}=M_1+M_2$. The shearing of the central zone C of the specimen leads to a moment M_1 and the shearing of the zone B lead to a moment M_2. Denoting L_b the length of the bar AB, the equilibrium of ABD leads to $A_x=0$ (Fig. 10). The equilibrium of AB leads to:

$$B_x = 0 \quad \text{and} \quad B_y = M_{12}/L_b\sin\left(^{\alpha}/_2\right) \quad (7)$$

Taking into account that $\ell = \sqrt{2}L_b$ *and* $\frac{\alpha}{2}=\frac{\pi}{4}-\frac{\gamma}{2}$, the load F on the machine is,

$$F = \frac{\ell}{\cos\frac{\gamma}{2} - \sin\frac{\gamma}{2}}\left(M_s(\gamma) + M_s\left(\frac{\gamma}{2}\right)\right) \quad (8)$$

This is consistent with equation (4) when $L=2\ell$.

Cauchy stress components

In the bias-extension test the textile specimen is considered as a continuum. Consequently the internal loads within the material can then be represented by a stress tensor. The components of this tensor, especially the shear stress components can be an alternative to the shear load and shear moment to quantify the internal shear efforts in the materials. The mechanical behavior of a woven textile material is strongly dependent on directions of directions of the warp and weft yarns. Consequently the basis defined by these yarn directions are preferred to express the stress tensor components and the mechanical behavior of the textile material. These fibre directions do not remain perpendicular during the

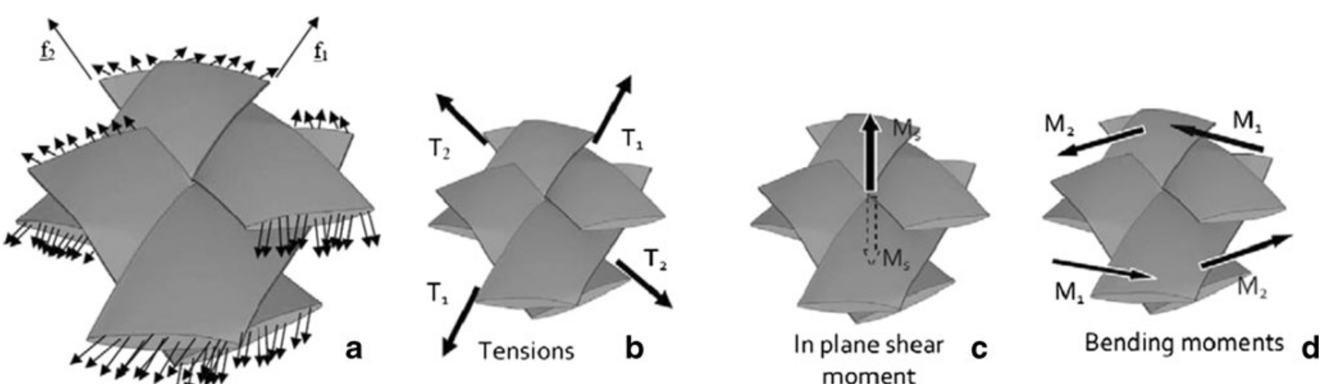

Fig. 9 (**a**) Loads on a unit woven cell and resultants: (**b**) tensions, (**c**) in-plane shear moment, (**d**) bending moments

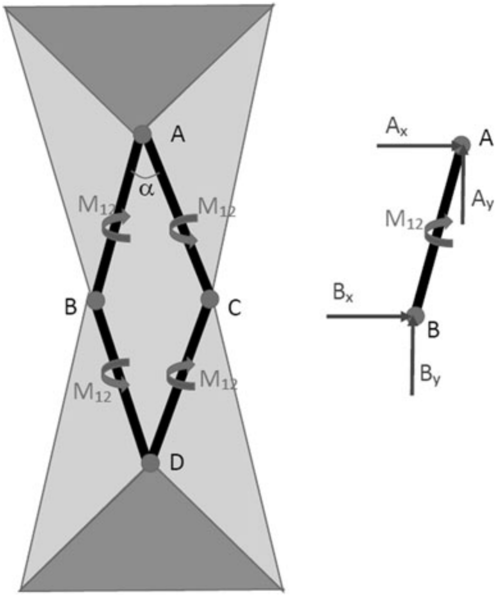

Fig. 10 Static analysis of the bias-extension test

reinforcement deformation especially in the bias-extension test. Consequently, there are different variances for the stress components in the frame defined by warp and weft yarns. The relationships between these components and the exterior applied loads can be determined but are not straightforward [46].

The curvilinear material coordinates ξ^1 and ξ^2 (Fig. 11) along warp and weft yarns define the material covariant base vectors at point M:

$$\underline{g}_1 = \frac{\partial \underline{OM}}{\partial \xi^1} \quad \text{and} \quad \underline{g}_2 = \frac{\partial \underline{OM}}{\partial \xi^2} \tag{9}$$

The associated contravariant base vectors $\underline{g}^\alpha$ are such as :

$$\underline{g}_\alpha \cdot \underline{g}^\beta = \delta_\alpha{}^\beta \tag{10}$$

Where α, β, are indices taking the values 1 or 2 and $\delta_\alpha{}^\beta$ is the Kronecker symbol. The covariant, contravariant and mixed components of the Cauchy stress tensor in the frames defined by the material covariant base vectors $\underline{g}_\alpha$ and contravariant base vectors $\underline{g}^\alpha$ are considered [47]:

$$\underline{\underline{\sigma}} = \sigma_{\alpha\beta}\ \underline{g}^\alpha \otimes \underline{g}^\beta = \sigma^{\alpha\beta}\ \underline{g}_\alpha \otimes \underline{g}_\beta = \sigma_\alpha{}^\beta\ \underline{g}^\alpha \otimes \underline{g}_\beta$$
$$= \sigma^\alpha{}_\beta\ \underline{g}_\alpha \otimes \underline{g}^\beta \tag{11}$$

⊗ denotes the tensorial product [47]. Denoting $\underline{n}_\alpha$ and $\underline{n}^\alpha$ the unit normal vectors in $\underline{g}_\alpha$ and $\underline{g}^\alpha$ directions, and dS_{n_α}, dS_{n^α} the corresponding elementary surface, the elementary force vector $\underline{dF}_{n_\alpha}$ on dS_{n_α} has two components, the first one, denoted dT_{n_α}, on the normal $\underline{n}_\alpha$ in the material direction α, the second one, denoted dR_{n_α}, in the perpendicular direction $\underline{n}^{3-\alpha}$ (Fig. 11) [46]:

$$\underline{dF}_{n_\alpha} = dT_{n_\alpha}\underline{n}_\alpha + dR_{n_\alpha}\underline{n}^{3-\alpha} = dT_{n_\alpha}\frac{\underline{g}_\alpha}{\left\|\underline{g}_\alpha\right\|} + dR_{n_\alpha}\frac{\underline{g}^{3-\alpha}}{\left\|\underline{g}^{3-\alpha}\right\|} \tag{12}$$

As,

$$\underline{dF}_{n_\alpha} = \left(\underline{\underline{\sigma}} \cdot \underline{n}_\alpha\right)\ dS_{n_\alpha} \tag{13}$$

The stress components in equation (11) can be related to dT_{n_α} and dR_{n_α}. These relations are given in [46]. In the case of a pure shear loading ($\underline{dT} = \underline{0}$), two sets of components ($\underline{\underline{\sigma}} = \sigma^{\alpha\beta}\underline{g}_\alpha \otimes \underline{g}_\beta$ and $\underline{\underline{\sigma}} = \sigma^\alpha{}_\beta \underline{g}_\alpha \otimes \underline{g}^\beta$) enable to obtain both null direct stresses and a direct relationship between the transverse load components and the transverse stresses. Thus, these frames and the corresponding stress components are those suited to analyze a pure transverse loading. For the others the pure shear will lead to direct stress components.

In a textile material with two fibre directions the elementary section dS_{n^α} of normal $\underline{n}^\alpha$ is parallel to the fibres (3-α) (Fig. 12a). Consequently, these fibres do not exert any load on this section. The load on the section dS_{n^α} is only due to the

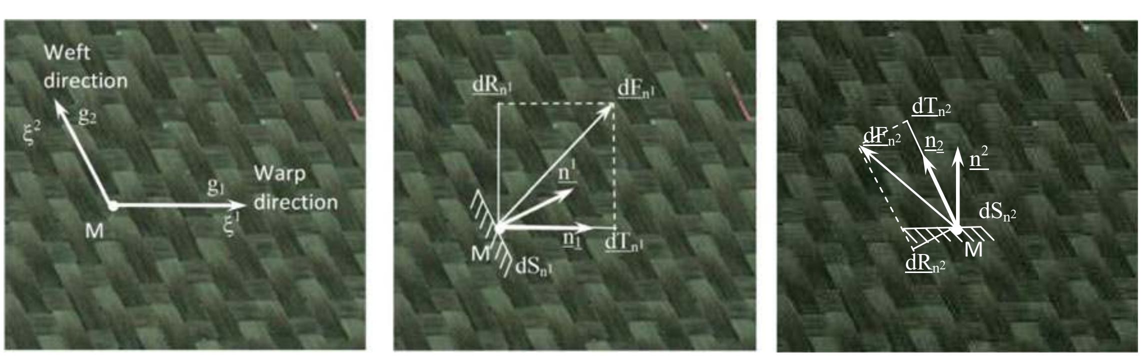

Fig. 11 Material coordinates, normal, elementary surfaces and elementary loads

Fig. 12 (**a**) Pure tensile loading (**b**) Pure in-plane shear loading

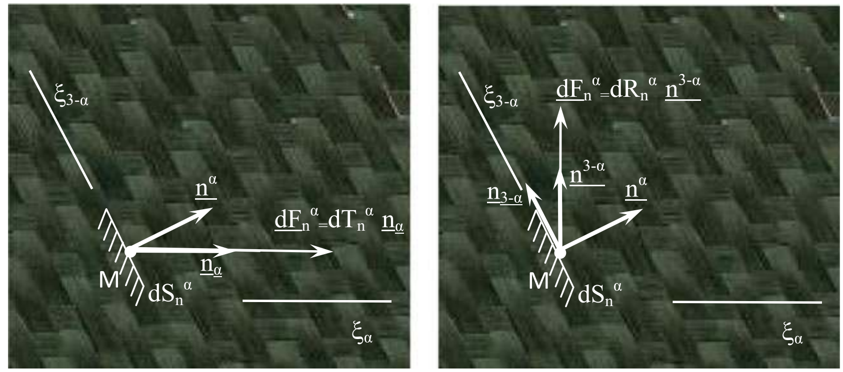

a Pure tensile loading **b** Pure in-plane shear loading

tension in the fibres α, $\underline{dF}_{n^\alpha} = dT_{n^\alpha}\underline{n}_\alpha$. A pure tensile loading is characterized by

$$dR_{n^\alpha} = 0 \ \ (\alpha = 1, 2) \tag{14}$$

The loads dT_{n^α} are the tension in the fibres α.

In the case of a pure in-plane shear loading the tensions in the fibres are equal to zero (Fig. 12b):

$$dT_{n^\alpha} = 0 \ \ (\alpha = 1, 2) \tag{15}$$

In any case, because section dS_{n^α} of normal $\underline{n}^\alpha$ is parallel to fibres (3-α), the tensions of these fibres do not contribute to $\underline{dF}_{n^\alpha}$. dT_{n^α} is the tensile load in fibres α. dR_{n^α} is the in-plane shear load. In textile materials, in a pure tensile state there are only loads in the fibre directions. In a pure shear state, the tensions are equal to zero. Denoting ℓ the specimen width (Fig. 4) and e its thickness, in the central zone, the static equilibrium leads to [46]:

$$\sigma_1{}^2 = \sigma_2{}^1 = \frac{F\left(\cos\frac{\gamma}{2} - \sin\frac{\gamma}{2}\right)}{\sqrt{2}\ e\ \ell} \tag{16}$$

Finally, the shear stress components can be considered as results of a bias-extension test. Nevertheless, only two variances ($\underline{\underline{\sigma}} = \sigma^{\alpha\beta}\underline{g}_\alpha \otimes \underline{g}_\beta$ and $\underline{\underline{\sigma}} = \sigma^\alpha{}_\beta \underline{g}_\alpha \otimes \underline{g}^\beta$) enable to obtain null direct stresses. The fact that the vectors $\underline{g}_\alpha$ and $\underline{g}^\alpha$ are not normed and does not remain perpendicular during a shear test does not render the use of the stress components simple.

Energetic approach for the PK2 shear stress calculation

Eq. (16) gives the shear Cauchy stress $\sigma_1{}^2$ in function of the measured load on the specimen. Nevertheless the different variances of the Cauchy stress components (equation 11) can appear as few easy to use. As it has been done in Eq. (2) to (5), an energetic approach can be used in the initial configuration to determine the second Piola-Kirckkoff (PK2) shear stress component in function of the global tensile load [48]. The kinematics of the bias-extension test gives the deformation gradient **F**.

$$\mathbf{F} = \sqrt{2}\sin\left(\frac{\pi}{4} - \frac{\gamma}{2}\right)\ \mathbf{e}_{10} \otimes \mathbf{e}_{10} + \sqrt{2}\cos\left(\frac{\pi}{4} - \frac{\gamma}{2}\right)\ \mathbf{e}_{20} \otimes \mathbf{e}_{20} \tag{17}$$

($\mathbf{e}_{10}, \mathbf{e}_{20}$) is the orthonormal frame where $\mathbf{e}_{20}$ is in the tensile direction (Fig. 4). Consequently the right Cauchy Green strain tensor $\mathbf{C} = \mathbf{F}^T\mathbf{F}$ and its time derivative $\mathbf{C}^{\cdot}$ are:

$$\begin{aligned} \mathbf{C} &= (1 - \sin(\gamma))\ \mathbf{e}_{10} \otimes \mathbf{e}_{10} + (1 + \sin(\gamma))\ \mathbf{e}_{20} \otimes \mathbf{e}_{20} \\ \dot{\mathbf{C}} &= \dot{\gamma}\cos(\gamma)(-\ \mathbf{e}_{10} \otimes \mathbf{e}_{10} +\ \ \mathbf{e}_{20} \otimes \mathbf{e}_{20}) \end{aligned} \tag{18}$$

The equality of internal and external power in a quasistatic test relates the load on the specimen F to the second Piola Kirckkoff stress **S**:

$$F\dot{d} = \frac{1}{2}\int_{\Omega_0} \mathbf{S} : \dot{\mathbf{C}}\, dV_0 \tag{19}$$

Taking into account the three zones A, B, C in the specimen with constant shear angle (Fig. 4)

$$F\dot{d} = \frac{1}{2} e\dot{\gamma}\left[S_c\cos\gamma(S_{22}(\gamma) - S_{11}(\gamma)) + \frac{1}{2}S_B\cos\frac{\gamma}{2}\left(S_{22}\left(\frac{\gamma}{2}\right) - S_{11}\left(\frac{\gamma}{2}\right)\right)\right] \tag{20}$$

where $S_{\alpha\beta}$ are the components of the PK2 stress tensor $S = S_{\alpha\beta}\mathbf{e}_{\alpha 0} \otimes \mathbf{e}_{\alpha 0}$ (α, β =1 or 2) in the frame ($\mathbf{e}_{10}, \mathbf{e}_{20}$). $S_{11}(\gamma)$ et $S_{22}(\gamma)$ are the diagonal stress components in the central zone C of the specimen and $S_{11}\left(\frac{\gamma}{2}\right)$ et $S_{22}\left(\frac{\gamma}{2}\right)$ those in zone B. Otherwise, Eq. 1 leads to:

$$\dot{\gamma} = \frac{\sqrt{2}\,d^{\cdot}}{D\sin\left(\frac{\pi}{4} - \frac{\gamma}{2}\right)} \tag{21}$$

Consequently, noting $S'_{\alpha\beta}$ the components of the PK2 stress tensor $S = S'_{\alpha\beta}\mathbf{f}_{\alpha 0} \otimes \mathbf{f}_{\alpha 0}$ (α, β =1 or 2) in the frame ($\mathbf{f}_{10}, \mathbf{f}_{20}$) in the initial directions of the yarns (Fig. 4), the shear stress component $S'_{12} = \frac{1}{2}(S_{22} - S_{11})$ can be calculated incrementally from the load on the specimen F.

$$S'_{12}(\gamma) = \frac{FD\left(\cos\left(\frac{\gamma}{2}\right) - \sin\left(\frac{\gamma}{2}\right)\right)}{2S_C e \cos\gamma} - \frac{S_B \cos\frac{\gamma}{2}}{4S_C \cos\gamma} S'_{12}\left(\frac{\gamma}{2}\right) \tag{22}$$

The inverse approach

In order to overcome the calculation of the force quantities defined in the previous sections, the inverse approach [49, 50] can be a way to identify the parameters relatives to in-plane shear of the used constitutive law. Finite element analyses of the bias-extension test are performed within an optimisation loop in order to determine the in-plane shear coefficients of the constitutive law that give the nearest F.E. analyses of the bias extension test. This approach avoids the use of the explicit relation between in-plane shear stresses and the load on the machine. Nevertheless this approach is not without drawback. In particular, the identified coefficients may depend on the initial values used for the simulation.

Bias-extension tests at high temperature

The in-plane shear tests are used to measure the shear properties of both dry composite reinforcements (used as preforms in the RTM process) and thermoset and thermoplastic prepregs. The in-plane behaviour of prepregs is significantly different from that of dry textile reinforcements. Depending on the state of the resin, the in-plane shear are substantially modified. Nevertheless the manufacturing process needs that in-plane shear stiffness is weak enough in order to achieve doubly curved shapes. In the case of thermoset prepregs, manufacturing and consequently the in-plane shear tests are performed before curing. In the case of thermoplastic prepreg, manufacturing and shear tests are performed at a temperature slightly over melting point. The in-plane shear tests must be performed at all the temperatures in the material processing range. The temperature may vary during the process and it is important that the actual properties are taken into account in a process simulation. Low temperature in a zone of a part during a thermoforming process can lead to a high shear stiffness and wrinkling [51]. The bias extension test can be used to test prepregs in the material processing range because the resin is weak enough in this case so that the fibres lead to the deformed shape of Fig. 4. This shape is due to inextensibility of the yarns and rotations at the yarn crossovers without slippage.

Some in-plane shear tests have been performed fairly soon within an oven [20, 31, 32]. A study of the effect of temperature on, in-plane shear behaviour of carbon satin/ Peek and carbon satin/ PPS prepregs using a bias-extension test has been made recently in [52]. The bias-extension test is compact and can be easily performed within an environmental chamber (Fig. 13). It nevertheless presents several difficulties. First the clamp of the specimen is difficult since its efficiency decrease when the matrix reach the melting point (Fig. 14a). The most important point is the necessity to have a constant temperature field in the specimen. If it is not the case the shear stiffness is not constant and the deformation of the specimen is no more those of the bias-extension test. Some zone, especially near the clamps that cool the specimen can remain undeformed (Fig. 14b). In addition it is not possible to wait a long time for a thermal equilibrium because the matrix are usually oxidized by high temperature and the test must be achieved in a matter of some minutes [53].

The bias-extension tests are carried out for temperatures on both sides of the manufacturing temperature. This temperature is slightly larger than melting temperature. The objective of these experiments is to account for the effect of the temperature on the prepreg properties in a forming simulation. A thermal analysis gives the temperature of the prepreg during the forming. This one may vary over the part. The resulting change of shear stiffness can affect the thermoforming process [51]. The loads on the specimen measured for bias-extension tests at temperature around the melting point (343 °C) for a carbon satin / PEEK matrix prepreg are shown Fig. 15. The influence of the temperature is strong. The in-plane shear stiffness is much larger at 320 °C than at 360 °C. Nevertheless over 360°, the shear stiffness does not decrease anymore because it is mainly those of the textile reinforcement.

In the case of the thermoplastic prepreg, the temperature is a main issue and the bias-extension tests must be done in function of the temperature. For these prepregs, the influence of the strain-rate can be tested using bias-extension test at different speeds. Figures 16 [8] and 17 [51] show the influence of the strain rate on in-plane shear force for two close prepreg with both PPS matrix. The influence of strain rate exists, but it is less important than the influence of temperature. Depending on the process it can be taken into account in the constitutive model or neglected [54, 55].

Influence of the tensions; biaxial bias-extension test

When a textile reinforcement is submitted to tension, the in-plane shear stiffness is increased. The influence of tension on in-plane shear behaviour has been investigated in the picture frame test [30, 33, 56] and by modelling approaches [57]. In the picture frame test it is possible (although technically

Fig. 13 Bias-extension test on a thermoplastic prepreg in an environmental chamber [51]

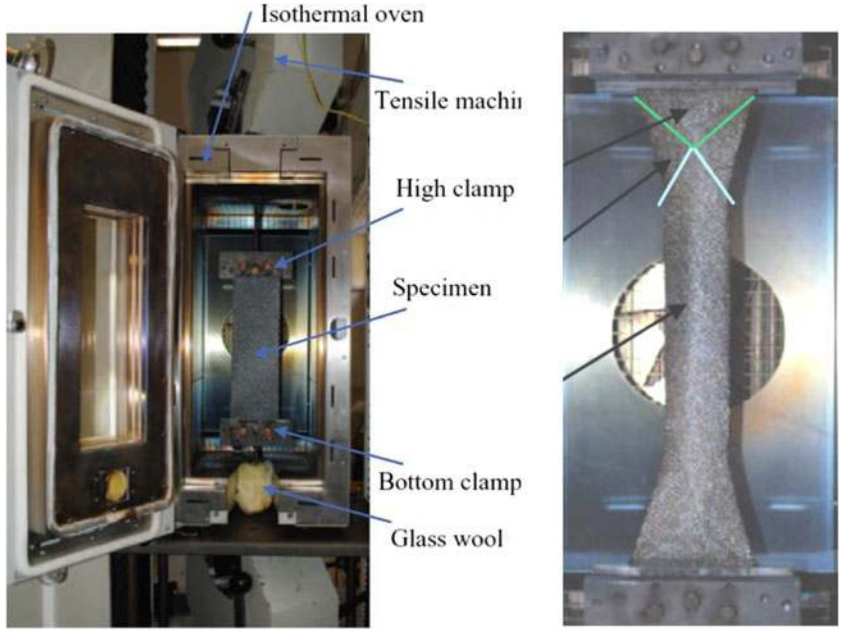

difficult) to add devices that impose tension in the yarns in addition to the in-plane shear prescribed by the picture frame. It has been shown that the influence of those tensions are important. In particular they strongly influence the onset of wrinkling [5, 58]. This is also a main difficulty of the standard picture frame test because it is difficult to avoid spurious tensions in the specimen that perturb the in-plane shear measurement [33]. On the other hand, in the bias-extension test the yarns have one or two free extremities. Consequently the tensions in the yarns are small and they don't disrupt the in-plane shear measurement. It is a main advantage of this test. The bias-extension test have been modified to analyse the shear-tension coupling. The biaxial bias-extension test is shown in Fig. 18 [58–60]. The objective of this test is to characterize wrinkling onset and tension in-plane shear coupling for woven textile reinforcements. Nevertheless the kinematics of the test is not simple and the use of this test needs to be strengthened.

Slippage mechanism during the bias-extension test

A main advantage of the bias-extension test is that the extremities of the yarns are free and consequently that there is no (or small) tension in the yarns. On the other hand the reinforcement is weakly held in position. The kinematics of the test is based on weaving that ensures that the cross over points act as fixed pin-jointed nodes. When the shear angles are large, slippage between the warp and weft yarns occurs. It is a weakness of the bias-extension test. This slippage has been analysed from the first studies on the bias-extension test [21, 22, 61]. Wang et al. observed that the slippage

Fig. 14 (a) Sliding of heels. (b) Inhomogeneity of temperature and fusion (c) The bias extension test shape is not achieved because of slippage in the jaws

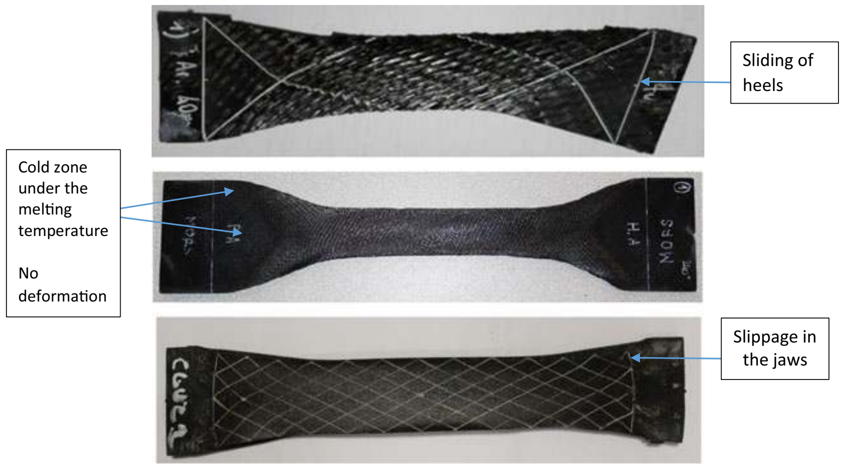

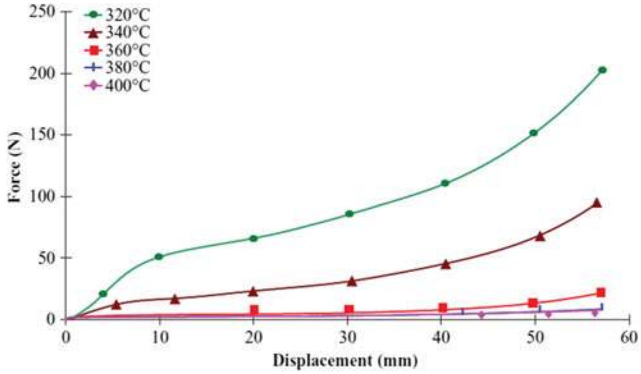

Fig. 15 Bias-extension test load in function of the temperature [52]

occurs mainly near the frontiers of the zones with constant in-plane shear (Fig. 19). Actually the importance of the slippage during a bias-extension test depends on the cohesion provided by the weaving (or the stitching for NCF materials). Figure 20 shows the shear angle versus displacement for two composite reinforcements (a glass plain woven textile pattern [62] and a G1151 interlock carbon fabric (manufactured by Hexcel) [63]). The theoretical angle (equation 1) obtained from the specimen extension is compared to the angle measured with a camera. For shear angles inferior to 40°, the agreement between theoretical and measured shear angles is good. Over 40°, slippage between yarns occurs and the measured angles are smaller than the theoretical ones [62, 63]. Depending on the fabric and on the cohesion due to the weaving, the angle from which the slippage is significant (40° for the G1151) can differ and can be smaller. Anyway, even if there if some slippage, the bias-extension test can be used to measure the in-plane shear properties but the shear angle must be measured independently of the grip displacement. This is in particular possible by using optical strain measurements.

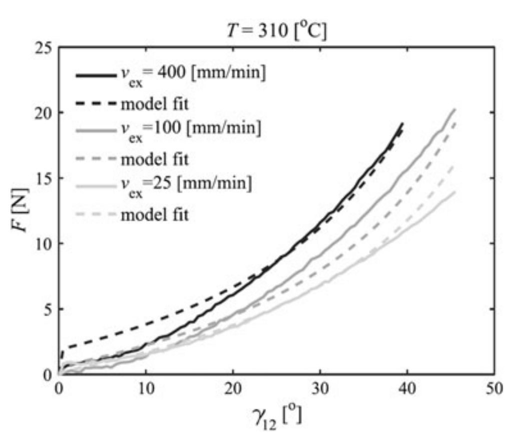

Fig. 16 Bias-extension tests at different rates on a PPS glass fabric prepreg [7]]

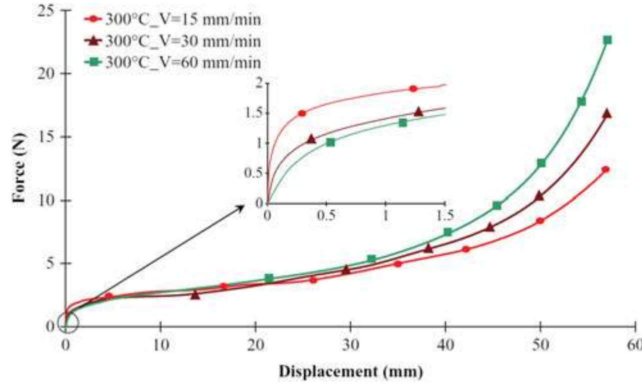

Fig. 17 Load versus displacement curves for carbon/PPS prepreg at 300 °C for different displacement rates [51]

Bias-extension test on NCF reinforcements

Among the textile composite reinforcements, the NCF (Non Crimp Fabrics) are made of continuous parallel fibres linked by stitching. They are made of one (UD-NCF), two (biaxial NCF) or three (triaxial NCF) direction of fibres that are linked by stitching. The biaxial NCF are the more common (Fig. 21). They have two directions of fibres (that are initially orthogonal) as woven reinforcements. As stated in their name, the fibres are straight (non crimp) and they avoid the loss of stiffness and strength due to yarn crimp. In the other hand the stitching insures a cohesion to the reinforcement that can be formed on double curved shapes [6, 63–66]. As the bias-extension test of woven material is based on the assumption that there is no slip between warp and weft yarns, one can ask whether the bias-extension test is possible for NCF. This depends on the stitching pattern. If the stitching insures a sufficient link between the two fibre directions of the biaxial NCF and allows the rotation between warp and weft yarns, it plays the role of the weaving. In this case the bias-extension test

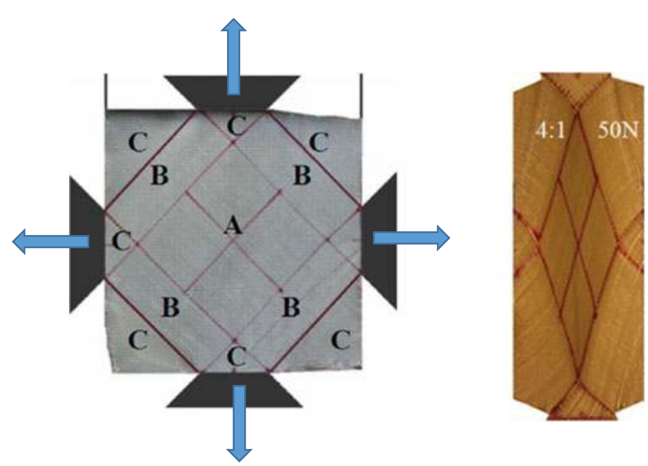

Fig. 18 The biaxial extension test (a) initial state (b) Deformed state [58]

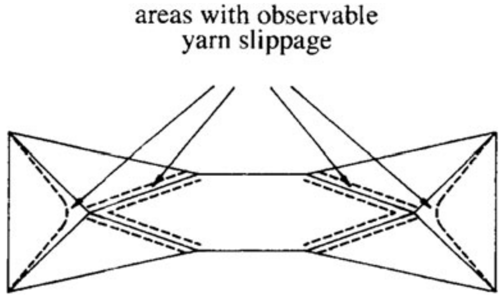

Fig. 19 Indication of slippage areas in a bias-extension test specimen [21]

can be considered to measure the NCF in-plane shear properties [63, 64, 66, 67]. The in-plane shear angle is defined as the change in angle between the fibres of the two layers (initially orthogonal). It can be measured using two synchronised cameras, one on each side of the specimen [63]. For a given axial displacement of the grips of the tensile machine, the measured angle are smaller than the theoretical angle given by equation (1). For example, for the NCF shown in Fig. 21, there is a difference about 30 % between the theoretical angle (equation (1)) and the angle measured with the two cameras (Fig. 22)[63]. The theoretical kinematic is nor more valid, the non-slippage assumption between the two plies is not verified. An analysis of the deformation

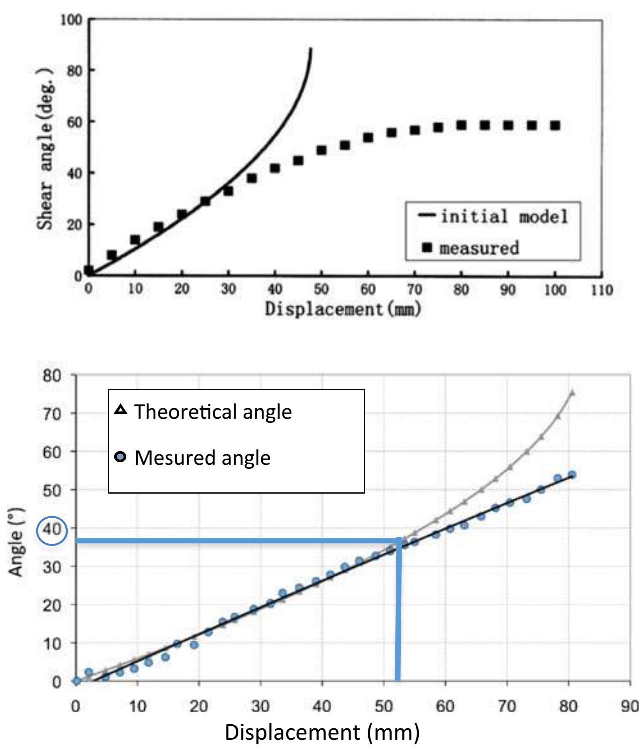

Fig. 20 Theoretical and measured shear angle during a bias-extension test (**a**) Glass plain woven textile pattern [62] (**b**) G1151 interlock carbon fabric [63]

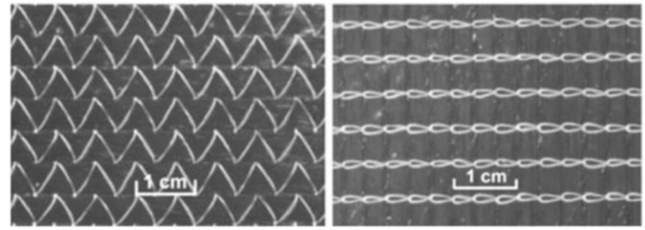

Fig. 21 NCF warp yarns side, NCF weft yarns side

of the bottom of the specimen shows some local slip that are shown Fig. 23. Consequently it is not possible to use the theoretical equations given in (1) to (5) and based on the non-slippage assumption. It is necessary to use the shear angle measured by the two synchronised cameras.

In [64] the bias-extension test of NCF is analysed by a mesoscopic approach. The yarns are modelled by 3D finite elements and the stitches by bar elements. This analysis allows frictional sliding between the yarns and the stiches. It leads to results that are in good agreement with the experimental deformation. However a mesoscopic analysis is not a simple way to analyse a bias-extension test. The mesoscopic approach of the bias-extension test will be detailed in a next section.

The slippage between the two plies of a biaxial NCF is often important in a forming process. The simulation of this process must take this slippage (some cm) into account [63].

The UD-NCF are sewed unidirectional non crimp fabric. They are closer to UD reinforcements than to woven fabrics. There is a single direction of parallel continuous fibres in the material. Bias-extension tests have been performed on such UD-NCF [68]. The deformed shape is far enough of the theoretical shape of the bias-extension test, but it is interesting to understand the deformation modes of the material. Some specific

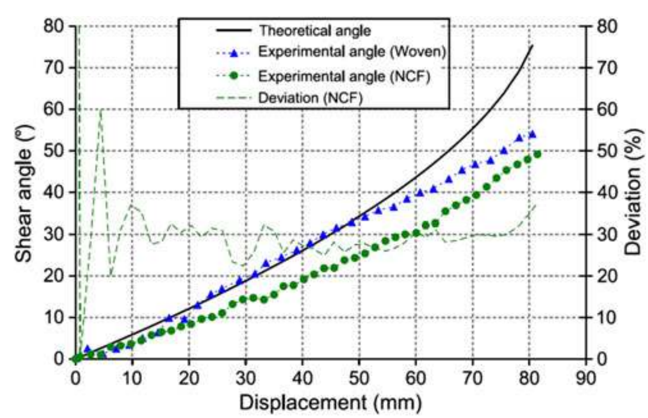

Fig. 22 Bias-extension test on a NCF. Comparison between theoretical and experimental shear angle versus displacement of the grip. Angle deviation from theoretical angle (dashed line) [63]

Fig. 23 Deformation of the bottom of the NCF specimen. Simplification of the deformation [63]

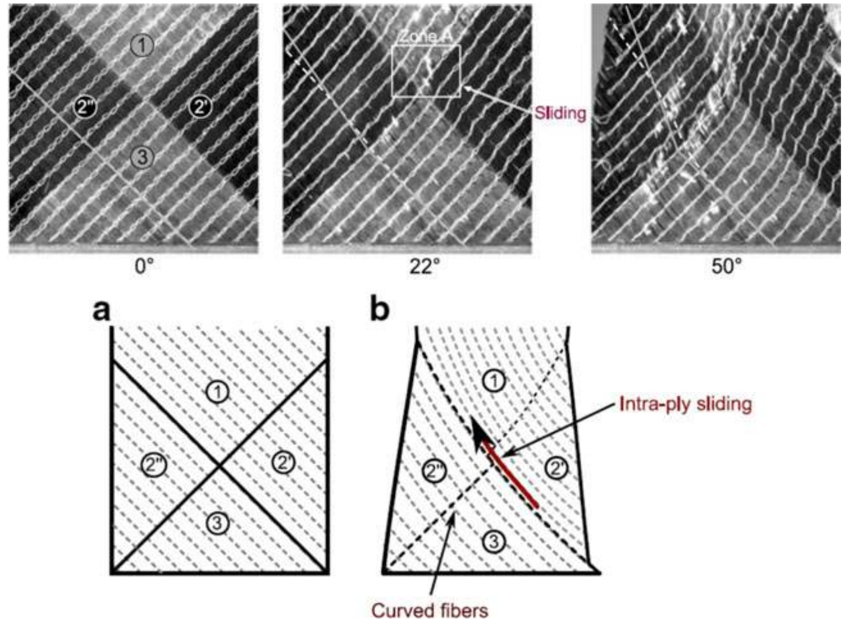

developments will be necessary to use this test to determine the in-plane shear properties of UD-NCF.

Numerical difficulties in the simulation of the bias-extension test. tension locking

The simulation of the bias-extension test needs to be perform at finite strain with material non-linearities. The approach can be implicit or explicit [7, 8, 64, 69]. A specific numerical problem which is a locking phenomenon has been highlighted [70–72]. In the bias-extension test, fibre yarns are oriented at ±45° to the specimen axis. Since the specimen is rectangular, the simplest mesh is obtained by a regular division into square or rectangular four node elements as in Fig. 24a. The result of the simulation is not correct. The obtained shape (Fig. 24b) is not those of the bias-extension test (Fig. 4). The computed load on the specimen is strongly overestimated (Fig. 24c). In the other hand, a mesh oriented in the fibre direction gives a correct result (Fig. 25). This problem is due to the very large tensile stiffness of the woven reinforcement in the warp and weft yarn directions. This leads to quasi inextensibility conditions in warp and weft directions at each Gauss point. As there are four gauss points per quadrangular element, the eight inextensibility conditions (two fibre directions at each Gauss point) cannot be verified as there are only two displacement degrees of freedom in a four node element (on average). This leads to locking called the tension locking. When the yarns are aligned with the element sides, the inextensibility equations in

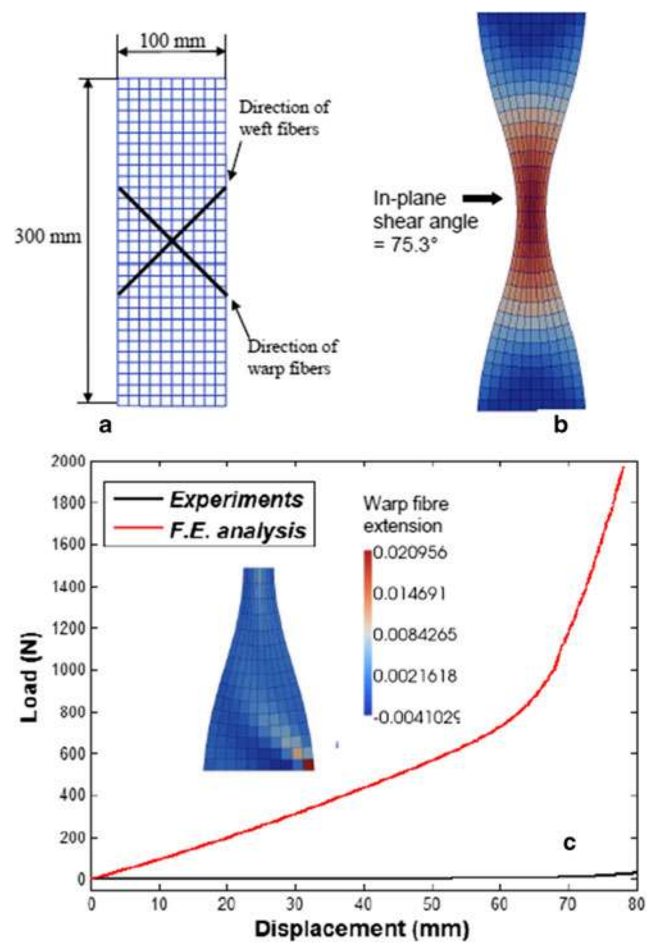

Fig. 24 (**a**) Initial mesh aligned with the specimen. The fibers are oriented at ± 45° (**b**) Deformed mesh for a 65 mm displacement (**c**) Load on the tensile machine obtained by simulation and by experiments and fibre extensions [72]

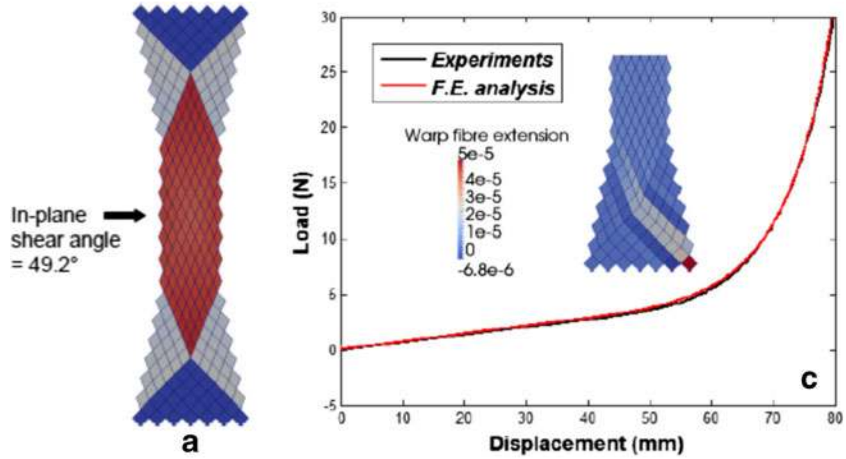

Fig. 25 (**a**) Simulation with a mesh aligned with the yarns (**c**) Load versus displacement curve obtained with an aligned mesh and fibre extensions [72]

the different Gauss points are identical and there can be verified. There are many cases of locking in finite element analyses: locking of incompressible materials [73], of transverse shear locking of C^0 plate or shell elements when the thickness small [74] among other locking phenomena [75]. Under-integration can be a solution to locking in particular to tension locking. The number of inextensibility constraints per quadrangle decrease to two and solutions exist. Nevertheless spurious singular modes can develop without deformation energy. The stabilization of these hourglass modes is necessary. A specific stabilization method has been developed in [72]. It is based on a Γ-projection method. It only acts on the non-constant part of the in-plane shear strains. This approach is numerically efficient. It is shown that locking is eliminated in the case of four node elements. Figure 26 shows that a rectangular mesh based on the specimen sides gives a correct solution when the method is used. Some multi-field finite elements have been proposed in order to avoid tension locking in [71].

Fiber bending stiffness and second gradient continuum

The idealized kinematics of the bias-extension test has been presented in Fig. 4. It is made of 7 zones of 3 types (A,B,C) with constant in-plane shear in each of them. This corresponds to a pin-joint kinematics. It is assumed that a continuous fibre has a constant orientation in each of these zones with a sharp change between zones. On the other hand, it is shown Fig. 27 that the change of direction is not instantaneous but that a transition area can be observed (Fig. 27b) (highlighted by means of two yellow lines). Such transition area is due to the bending stiffness of the fibres that lead to a curvature radius between the two zones with a different fibre direction (C and B on Fig. 27b). The kinematics based on the pin-joint assumption described at the beginning of the paper leads to different and constant directions of the fibres in zone A, B, C. The experimental observations, on the other hand, show that the bending stiffness of the fibres actually leads to transition areas. These zones cannot be described by the pin-joint

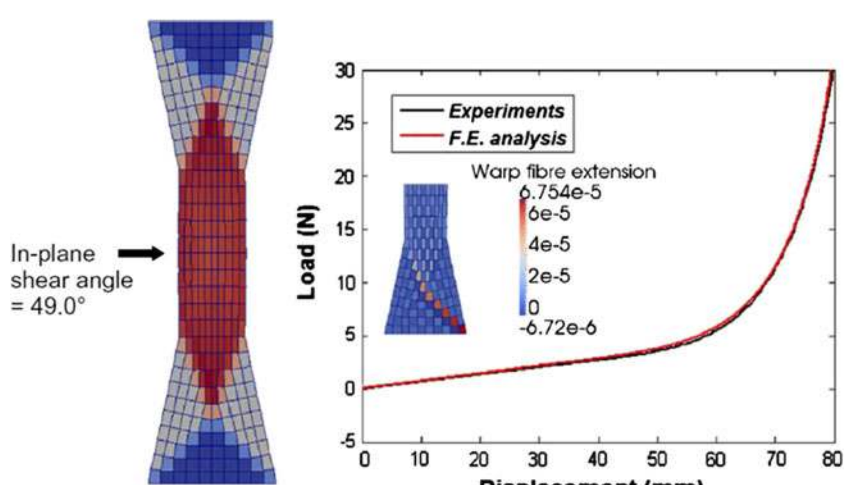

Fig. 26 (**a**) Simulation with a mesh aligned with the specimen using the stabilization approach (**c**) Load versus displacement curve obtained with an aligned mesh and fibre extensions [72]

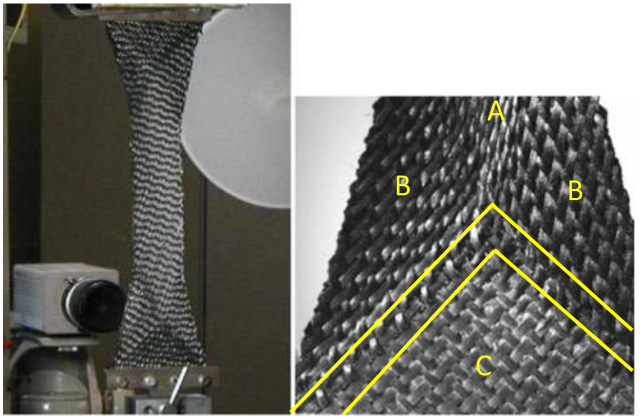

Fig. 27 Transition layer between the zones with constant shear in a bias-extension test

kinematics nor by a classical continuum approach. In order to describe these zones, a generalized continuum theory may be used. A second gradient hyperelastic orthotropic continuum theory for fibrous materials has been developed in [76, 77]. The strain energy density depends both of the Right Cauchy-Green deformation tensor $\mathbf{C} = \mathbf{F}^{\mathrm{T}}\,\mathbf{F}$ and of its gradient $\nabla\mathbf{C}$ ($\mathbf{F}$ is the deformation gradient tensor).

$$W(\mathbf{C}, \nabla\mathbf{C}) = W_I(\mathbf{C}) + W_{II}(\nabla\mathbf{C}) \tag{23}$$

W_I is the first gradient strain energy, W_{II} is the second gradient strain energy. Definitions and identifications of the first gradient strain energies for different fibrous reinforcements can be found in [78, 79] and of the second gradient strain energy in [76, 77, 80]. The simulation of the bias-extension test based on the strain energy with a second gradient part (equation 22) shows the transition areas that have been highlighted at the frontiers of the zones A, B, C (Fig. 28).

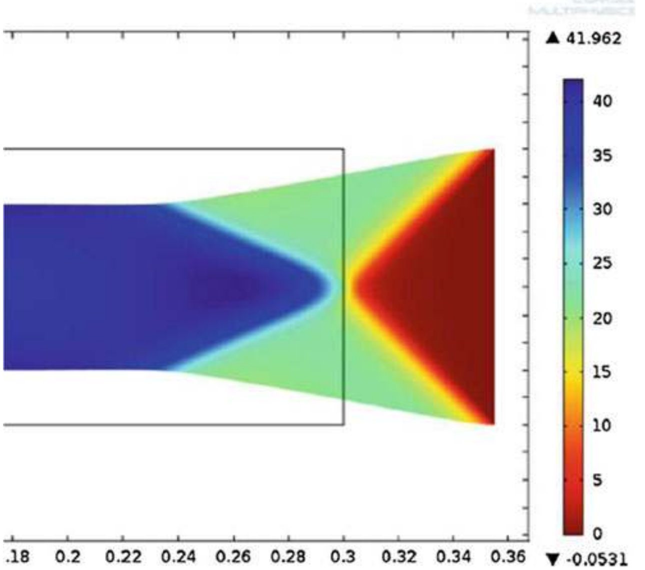

Fig. 28 Simulation of a bias-extension test base on a second gradient theory. Transition layers for the shear angle. [76]

More generally, the second gradient approach is a way to take into account the local bending stiffness of the fibres. This cannot be described by classical continuum mechanical models. However the implementation of these models into numerical codes shows some difficulties which are being recently studied by means of other methods [81, 82]. Another way to account for the local fibre bending stiffness is the introduction of a rigidity related to the curvature in continuum finite element [83]. A detailed generalised plate model including geodesic bending energy, i.e. energy related to second gradient in-place displacement, has been recently developed in [84–86].

Bias extension test on an unbalanced woven reinforcement

A significant part of the textile composite reinforcements are unbalanced. Warp yarns are much larger than weft yarns. The strong warp yarns withstand the loads in the composite part. The small weft ones ensure the cohesion of the reinforcement. The importance of the in-plane bending stiffness of the fibres that have been highlighted in the previous section and has been shown to be significant in the case of balanced fabric becomes even more important for unbalanced reinforcements. In particular, it has been shown that the asymmetric S-shape obtained when an unbalanced reinforcement (Fig. 29) subjected to a bias extension test (Fig. 30) is due to the very different in-plane bending stiffness of the warp and weft yarns [87, 88]. In order to account for most fundamental deformation mechanisms occurring in unbalanced reinforcements, a second gradient, hyperelastic, initially orthotropic continuum model has been introduced in [87, 88]. The deformed shape obtained from this approach shows a good agreement with the experiment (Figs. 30 and 31). It can be seen that the S-shape is due to

Fig. 29 Unbalanced fabric

Fig. 30 Experimental S-shape [87]

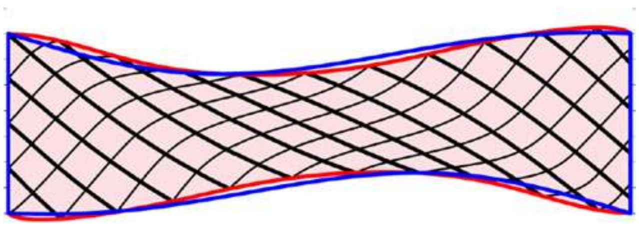

Fig. 31 Simulation of the deformation using a second gradient approach [87]

very different curvatures of the warp and weft yarns in the deformed configuration.

Mesoscopic analysis

It has been seen above that slippage occurs in a bias-extension test especially for large shear angles. It can even happen for smaller angles when the cohesion between warp and weft fibres is weak. This is the case for most NCF reinforcements as shown above. In this case, the continuum mechanic approaches are no more valid. In a mesoscopic approach each yarn is considered as a solid in contact and possible sliding with friction with its neighbours. The yarn is modelled as a continuous material with a specific mechanical behaviour in order to take into account that it is made of many (thousand) fibres. It is not a completely discrete modelling as the so called microscopic approach where each fibre is modelled by a beam element in contact-friction with the other fibres [89]. The mesoscopic approach allows to simulate the sliding between the yarns (and the stitch in case of a NCF). Consequently the simulation of the bias-extension test in case of slippage is possible. The F.E. model used to described a woven cell must be simple enough to permit the computation of the whole reinforcement. Figure 32 shows a simplified unit woven cell where the yarns are described by shell finite elements [90]. Contact with Coulomb friction between the elements is considered. The mechanical constitutive model of the yarn must take into account that it is made of thousands of fibres. Both specific hypoelastic [91–93] and hyperelastic [78, 94] laws have been developed. The bending stiffness of the shell elements is not related to the membrane stiffness because of the fibrous nature of the yarn. It is directly measured by a cantilever bending test [95, 96]. Figure 33 compares the

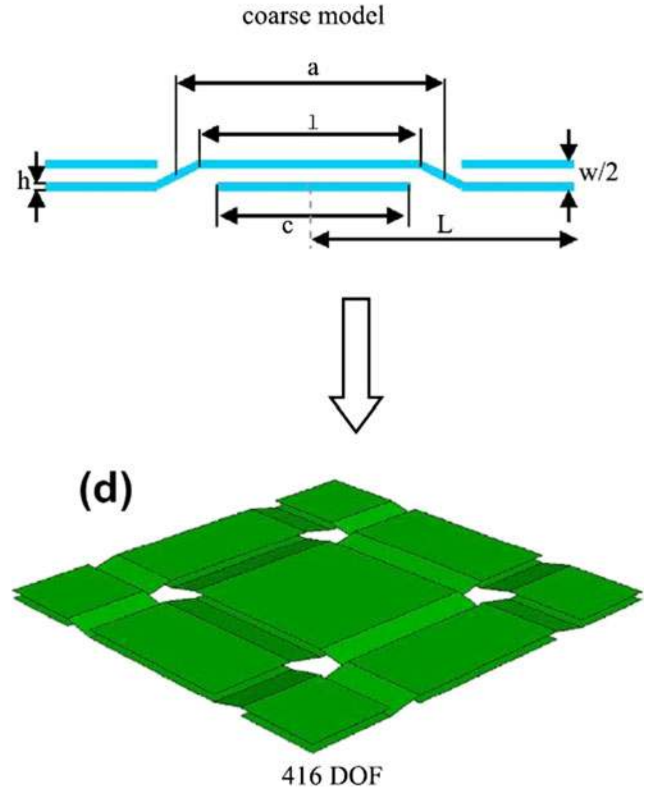

Fig. 32 The mesoscopic model of unit cell of plain weave

experimental deformation of a bias-extension test on a glass plain weave specimen with the result of a mesoscopic simulation and with the theoretical shape based on the pin joint assumption. Up to 40° both theoretical and mesoscopic approach give shear angles in correct agreement with the experiments. Over 40° slippage occurs and the experimental shear angle is smaller than the theoretical one. The mesoscopic simulation using shell elements is on correct agreement and tracks the sliding of the yarns over 40°. Membrane elements give poor results because the lack of bending stiffness leads to underestimated normal contact loads and consequently underestimated friction loads and too large sliding.

A mesoscopic simulation of the bias-extension test for NCF reinforcements is done in [64]. The yarns are model by solid elements and the stitches by bar elements. Yarns and stitches are in contact with friction. The analysis of fibre slip in the specimen is analysed by the mesoscopic model and compare to experiments. Other mesoscopic analysis are presented in [97]. Meso modelling is an accurate approach to analyse the bias-extension test. These simulations allow to track the yarn slip. Nevertheless, the finite element models are complex with many contacts with friction. They must be used when the classical pin joint assumption for the bias extension test is not satisfactory.

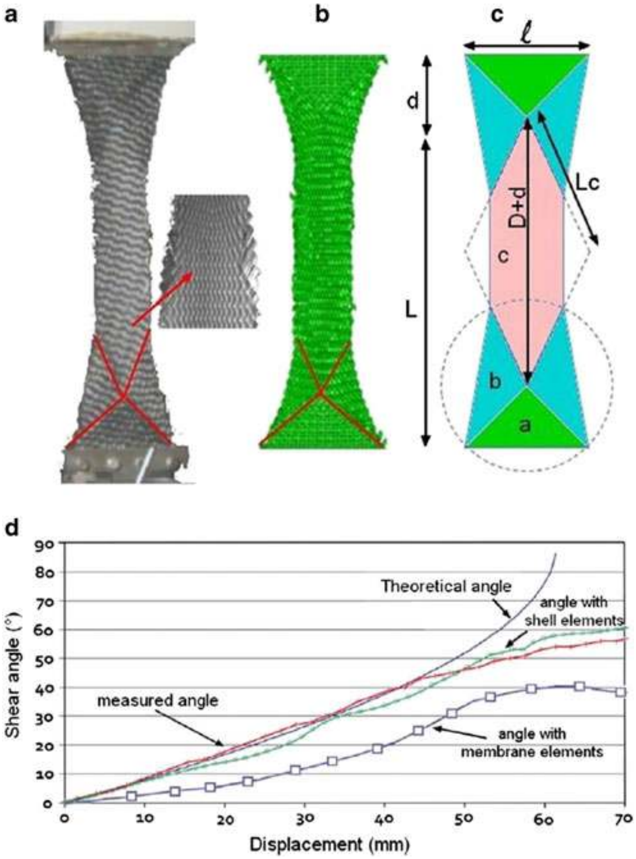

Fig. 33 Bias-extension test for 58° shear angle with local sliding (**a**) experiments, (**b**) corresponding mesoscopic finite element simulation. (**c**) pin-joint kinematics (**d**) Shear angle as a function of displacement, including theory (Eq. (1)), experimental test, and simulations with shell and membrane elements [90]

Conclusion

The bias-extension test is one of the two main experiments used to determine the in-plane shear properties of textile materials and in particular of continuous fibres composite reinforcements. The test is rather simple as it consists of a tensile test on a rectangular specimen where the fibres are oriented at 45°. The yarns have all one or two free edges and the test avoids spurious tensions in the fibres. This is an important advantage. Nevertheless it is a test on a very anisotropic material, at finite strains with large rotations of the fibres. It is driven by the quasi-inextensibility of the fibres. Research work on this test have been and are numerous. A first approach based on the absence of slippage at crossover and fibre inextensibility gives basic kinematics and shear load relations. The internal actions due to shear are represented by shear loads, shear moments, shear stresses but there is not a unified point of view on these quantities.

Beyond the above basic assumptions there are several aspects that must be better analysed in the bias-extension tests. Possible slippage is one of the weak point of the test. It is necessary to know when it happens, rendering obsolete the basic assumptions and the associated equations. The analysis of the bias-extension test with slippage can be possible in particular thanks to optical measures. The in-plane bending stiffness of the fibres modifies the theoretical zones with constant shear of the bias-extension test. This test may be a way to measure bending stiffness of the yarns. Meso F.E. modelling enables to analyse and model the bias-extension test beyond the basic assumptions. Slippage between the yarns, tension in the yarns, bending stiffness can be analyzed through this approach. The bias-extension test is one of the main in-plane shear test for composite reinforcements. Many work has been carried out concerning this test. Nevertheless many progresses are possible beyond the basic assumption generally used. Indeed microscopic complexity of considered mechanical systems may require for their macro modelling the introduction of richer continuum models.

References

1. Wang P, Legrand X, Boisse P, Hamila N, Soulat D (2015) Experimental and numerical analyses of manufacturing process of a composite square box part: comparison between textile reinforcement forming and surface 3D weaving. Compos Part B 78:26–34
2. Prodromou AG, Chen J (1997) On the relationship between shear angle and wrinkling of textile composite preforms. Compos Part A 28A:491–503
3. Skordos AA, Aceves CM, Sutcliffe MP (2007) A simplified rate dependent model of forming and wrinkling of pre-impregnated woven composites. Compos A: Appl Sci Manuf 38(5):1318–1330
4. Hallander P, Akermo M, Mattei C, Petersson M, Nyman T (2013) An experimental study of mechanisms behind wrinkle development during forming of composite laminates. Compos A: Appl Sci Manuf 50:54–64
5. Boisse P, Hamila N, Vidal-Sallé E, Dumont F (2011) Simulation of wrinkling during textile composite reinforcement forming. influence of tensile, in-plane shear and bending stiffnesses. Compos Sci Technol 71:683–692
6. Yu WR, Harrison P, Long A (2005) Finite element forming simulation for non-crimp fabrics using a non-orthogonal constitutive equation. Compos Part A 36:1079–1093
7. Hamila N, Boisse P, Sabourin F, Brunet M (2009) A semi-discrete shell finite element for textile composite reinforcement forming simulation. Int J Numer Method Eng 79:1443–1466
8. Haanappel SP, ten Thije RHW, Sachs U, Rietman B, Akkerman R (2014) Formability analyses of uni-directional and textile reinforced thermoplastics. Compos Part A: Appl Sci Manuf 56:80–92
9. Smith JR, Vaidya UK, Johnstone JK (2014) Analytical modeling of deformed plain woven thermoplastic composites. Int J Mater Form 7(4):379–393
10. Hübner M, Rocher JE, Allaoui S, Hivet G, Gereke T, Cherif C (2015) Simulation-based investigations on the drape behavior of 3D woven fabrics made of commingled yarns. Int J Mater Form. doi:10.1007/s12289-015-1245-8

11. Bickerton S, Šimáček P, Guglielmi SE, Advani SG (1997) Investigation of draping and its effects on the mold filling process during manufacturing of a compound curved composite part. Compos A: Appl Sci Manuf 28(9):801–816
12. Gascón L, García JA, LeBel F, Ruiz E, Trochu F (2015) A two-phase flow model to simulate mold filling and saturation in Resin Transfer Molding. Int J Mater Form. doi:10.1007/s12289-015-1225-z
13. Blais M, Moulin N, Liotier PJ, Drapier S (2015) Resin infusion-based processes simulation: coupled Stokes-Darcy flows in orthotropic preforms undergoing finite strain. Int J Mater Form. doi:10.1007/s12289-015-1259-2
14. Lopez E, Abisset-Chavanne E, Lebel F, Upadhyay R, Comas S, Binetruy C, Chinesta F (2015) Flow modeling of linear and nonlinear fluids in two and three scale fibrous fabrics. Int J Mater Form. doi:10.1007/s12289-015-1280-5
15. Lindberg J, Behre B, Dahlberg B (1961) Shearing and buckling of various commercial fabrics. Text Res J 31(2):99–122
16. Grosberg P, Park BJ (1966) The mechanical properties of woven fabrics, part V: the initial modulus and the frictional restraint in shearing of plain weave fabrics. Text Res J 36: 420–431
17. Grosberg P, Leaf GAV, Park BJ (1968) The mechanical properties of woven fabrics, part VI: the elastic shear modulus of plain weave fabrics. Text Res J 38(11):1085–1100
18. Spivak SM, Treloar LRG (1968) The behavior of fabrics in shear: part III: the relation between bias-extension and simple shear. Text Res J 38:963–971
19. Skelton J (1976) Fundamental of fabric shear. Text Res J 46(12): 862–869
20. McGuinness GB, O_Bradaigh CM (1997) Development of rheological models for forming flows and picture-frame shear testing of fabric reinforced thermoplastic sheets. J Non-Newtonian Fluid Mech 73:1–28
21. Wang J, Page JR, Paton R (1998) Experimental investigation of the draping properties of reinforcement fabrics. Compos Sci Technol 58:229–237
22. Page J, Wang J (2000) Prediction of shear force and an analysis of yarn slippage. Compos Sci Technol 60:977–986
23. Page J, Wang J (2002) Prediction of shear force using 3D non-linear FEM analyses for a plain weave carbon fabric in a bias-extension state. Finite Elem Anal Des 38:755–764
24. Potter K (2002) Bias-extension measurements on cross-plied unidirectional prepreg. Compos Part A 33:63–73
25. Cao J, Akkerman R, Boisse P, Chen J et al (2008) Characterization of mechanical behavior of woven fabrics: experimental methods and benchmark results. Compos Part A 39:1037–1053
26. Hu JL, Zhang YT (1997) The KES shear test for fabrics. Text Res J 67(9):654–664
27. Haanappel SP, Akkerman R (2014) Shear characterisation of unidirectional fibre reinforced thermoplastic melts by means of torsion. Compos Part A 56:8–26
28. Nguyen M, Herszberg I, Paton R (1999) The shear properties of woven carbon fabric. Compos Struct 47:767–779
29. Mohammed U, Lekakou C, Dong L, Bader MG (2000) Shear deformation and micromechanics of woven fabrics. Compos Part A: Appl Sci Manuf 31:299–308
30. Hivet G, Duong AV (2011) A contribution to the analysis of the intrinsic shear behavior of fabrics. J Compos Mater 45(6):695–716
31. Lebrun G, Bureau MN, Denault J (2003) Evaluation of bias-extension and picture-frame test methods for the measurement of intraply shear properties of PP/glass commingled fabrics. Compos Struct 61:341–352
32. Harrison P, Clifford MJ, Long AC (2004) Shear characterisation of viscous woven textile composites, a comparison between picture frame and bias-extension experiments. Compos Sci Technol 64: 1453–1465
33. Launay J, Hivet G, Duong AV, Boisse P (2008) Experimental analysis of the influence of tensions on in plane shear behaviour of woven composite reinforcements. Compos Sci Technol 68: 506–515
34. Mark C, Taylor HM (1956) The fitting of woven cloth to surfaces. J Text Instit 47:477–488
35. Van Der Ween F (1991) Algorithms for draping fabrics on doubly curved surfaces. Int J Numer Methods Eng 31:1414–1426
36. Cherouat A, Borouchaki H, Billoet JL (2005) Geometrical and mechanical draping of composite fabric. Eur J Comput Mech 14(6–7):693–708
37. Lomov SV, Boisse P, Deluycker E, Morestin F, Vanclooster K, Vandepitte D, Verpoest I, Willems A (2008) Full-field strain measurements in textile deformability studies. Compos Part A 39(8): 1232–1244
38. Pazmino J, Carvelli V, Lomov SV, Van Mieghem B, Lava P (2014) 3D digital image correlation measurements during shaping of a non-crimp 3D orthogonal woven E-glass reinforcement. Int J Mater Form 7(4):439–446
39. Zouari B, Daniel JL, Boisse P (2006) A woven reinforcement forming simulation method. influence of the shear stiffness. Comput Struct 84(5–6):351–363
40. Peng XQ, Cao J, Chen J, Xue P, Lussier DS, Liu L (2004) Experimental and numerical analysis on normalization of picture frame tests for composite materials. Compos Sci Technol 64:11–21
41. Harrison P, Wiggers J, Long AC (2008) Normalization of shear test data for rate independent compressible fabrics. J Compos Mater 42: 2315–2344
42. Härtel F, Harrison P (2014) Evaluation of normalisation methods for uniaxial bias-extension tests. Compos Part A 67:61–69
43. Cao J, Cheng HS, Yu TX et al. (2004) A cooperative benchmark effort on testing of woven composites, In: Proceedings of the 7th int. ESAFORM conference on material forming, Trondheim, Norway, p. 305–8
44. Hamila N, Boisse P (2007) A Meso–Macro three node finite element for draping of textile composite preforms. Appl Compos Mater 14:235–250
45. Hamila N, Boisse P (2008) Simulations of textile composite reinforcement draping using a new semi-discrete three node finite element. Compos Part B 39:999–1010
46. Hivet G, Vidal-Sallé E, Boisse P (2013) Analysis of the stress components in a textile composite reinforcement. J Compos Mater 47(3):269–285
47. Basar Y, Weichert D (2000) Nonlinear continuum mechanics of solids: fundamental mathematical and physical concepts. Springer Science & Business Media
48. Guzman-Maldonado E (2016) Modélisation et simulation de la mise en forme des matériaux composites préimprégnés à matrice thermoplastique et à fibres continues. Ph. D thesis, Université de Lyon
49. Marquardt DW (1963) An algorithm for least squares estimation of nonlinear parameters. J Soc Indus Appl Math 11(2):431–441
50. Schnur DS, Zabaras N (1992) An inverse method for determining elastic material properties and a material interface. Int J Num Meth Eng 33:2039–2057
51. Wang P, Hamila N, Boisse P (2013) Thermoforming simulation of multilayer composites with continuous fibres and thermoplastic matrix. Compos Part B: Eng 52:127–136
52. Wang P, Hamila N, Pineau P, Boisse P (2014) Thermomechanical analysis of thermoplastic composite prepregs using bias-extension test. J Thermoplast Compos Mater 27(5):679–698
53. Gupta YN, Chakraborty A, Pandey GD, Setua DK (2004) Thermal and thermooxidative degradation of engineering thermoplastics and life estimation. J Appl Polym Sci 92:1737–1748

54. Guzman-Maldonado E, Hamila N, Boisse P, Bikard J (2015) Thermomechanical analysis, modelling and simulation of the forming of pre-impregnated thermoplastics composites. Compos Part A 78:211–222
55. Guzman-Maldonado E, Hamila N, Naouar N, Moulin G, Boisse P (2016) Simulation of thermoplastic prepreg thermoforming based on a visco-hyperelastic model and a thermal homogenization. Mater Des 93:431–442
56. Nosrat-Nezami F, Gereke T, Eberdt C, Cherif C (2014) Characterisation of the shear–tension coupling of carbon-fibre fabric under controlled membrane tensions for precise simulative predictions of industrial preforming processes. Compos Part A 67: 131–139
57. Lomov SV, Verpoest I (2006) Model of shear of woven fabric and parametric description of shear resistance of glass woven reinforcements. Compos Sci Technol 66:919–933
58. Harrison P, Abdiwi F, Guo Z, Potluri P, Yu WR (2012) Characterising the shear–tension coupling and wrinkling behaviour of woven. Compos Part A 43:903–914
59. Sharma SB, Sutcliffe MPF, Chang SH (2003) Characterisation of material properties for draping of dry woven composite material. Compos Part A 34:1167–1175
60. Harrison P (2012) Normalisation of biaxial bias-extension test results considering shear tension coupling. Compos Part A 43(9): 1546–1554
61. Potter KD (1979) The influence of accurate stretch data for reinforcements on the production of complex structural mouldings. Composites 10:161–173
62. Zhu BA, Yu TX, Tao XM (2007) Large deformation and slippage mechanism of plain woven composite in bias-extension. Compos Part A 38:1821–1828
63. Bel S, Boisse P, Dumont F (2012) Analyses of the deformation mechanisms of non-crimp fabric composite reinforcement during preforming. Appl Compos Mater 19:513–528
64. Creech G, Pickett AK (2006) Meso-modelling of non-crimp fabric composites for coupled drape and failure analysis. J Mater Sci 41: 6725–6736
65. Lee J, Hong S, Yu W, Kang T (2007) The effect of blank holder force on the stamp forming behaviour of non-crimp fabric with a chain stitch. Compos Sci Technol 67(3–4): 357–366
66. Bel S, Hamila N, Boisse P, Dumont F (2012) NCF composite reinforcement preforming: Importance of inter-ply sliding. Compos Part A 43:2269–2277
67. Lomov SV, Barburski M, Stoilova TZ, Verpoest I, Akkerman R, Loendersloot R et al (2005) Carbon composites based on multiaxial multiply stitched preforms. part 3: biaxial tension, picture-frame and compression tests of the preforms. Compos Part A 36: 1188–1206
68. Schirmaier F, Weidenmann KA, Kaerger L, Henning F (2015) Characterization of the draping behaviour of sewed unidirectional non-crimp fabrics (UD-NCF). Compos Part A 80(2016):28–38
69. Boisse P, Bussy P, Ladeveze P (1990) A new approach in non-linear mechanics: the large time increment method. Int J Numer Method Eng 29:647–663
70. ten Thije RHW, Akkerman R (2008) Solutions to intra-ply shear locking in finite element analyses of fibre reinforced materials. Compos Part A 39:1167–1176
71. Yu X, Cartwright B, McGuckin D, Ye L, Mai YW (2006) Intraply shear locking in finite element analyses of woven fabric forming processes. Compos Part A 37:790–803
72. Hamila N, Boisse P (2013) Locking in simulation of composite reinforcement deformations. analysis and treatment. Compos Part A 53:109–117
73. Belytschko T, Bachrach WE (1986) Efficient implementation of quadrilaterals with high coarse-mesh accuracy. Comput Meth Appl Mech Eng 54:279–301
74. Dvorkin EN, Bathe KJ (1984) A continuum mechanics based four-node shell element for general nonlinear analysis. Eng Comput 1: 77–88
75. Belytschko T, Liu WK, Moran B et al. (2000) Non linear finite elements for continua and structures. John Wiley & Sons Inc
76. Ferretti M, Madeo A, dell'Isola F, Boisse P (2014) Modeling the onset of shear boundary layers in fibrous composite reinforcements by second-gradient theory. Z Angew Math Phys 65(3):587–612
77. d'Agostino V, Giorgio I, Greco L, Madeo A, Boisse P (2015) Continuum and discrete models for structures including (quasi-) inextensible elasticae with a view to the design and modeling of composite reinforcements, Int. J Solids Struct 59:1–17
78. Aimène Y, Vidal-Sallé E, Hagège B, Sidoroff F, Boisse P (2010) A hyperelastic approach for composite reinforcement large deformation analysis. J Compos Mater 44:5–26
79. Charmetant A, Orliac JG, Vidal-Sallé E, Boisse P (2012) Hyperelastic model for large deformation analyses of 3D interlock composite preforms. Compos Sci Technol 72: 1352–1360
80. Madeo A, Ferretti M, dell'Isola F, Boisse P (2015) Thick fibrous composite reinforcements behave as special second gradient materials: three point bending of 3D interlocks. Z Angew Math Phys 66(4):2041–2060
81. Cazzani C, Antonio MM, Turco E (2014) Isogeometric analysis: a powerful numerical tool for the elastic analysis of historical masonry arches. Contin Mech Thermodyn 28(1-2):139–156
82. Greco FL, Cuomo M (2015) An isogeometric implicit G1 mixed finite element for Kirchhoff space rods. Comput Methods Appl Mech Eng 298(1)2016, 325–349
83. Mathieu S, Hamila N, Bouillon F, Boisse P (2015) Enhanced modeling of 3D composite preform deformations taking into account local fiber bending stiffness. Compos Sci Technol 117:322–333
84. Dell'Isola F, Steigmann D (2015) A two-dimensional gradient-elasticity theory for woven fabrics. J Elast 118(1):113–125
85. Steigmann D, Dell'Isola F (2015) Mechanical response of fabric sheets to three-dimensional bending, twisting, and stretching. Acta Mech Sinica 31(3):373–382
86. Eremeyev VA, Holm A (2015) On the direct approach in the theory of second gradient plates, shell and membrane theories in mechanics and biology. Springer International Publishing, 147–154
87. Madeo A, Barbagallo G, D'Agostino MV, Boisse P (2016) Continuum and discrete models for unbalanced woven fabrics. Int J Solids Struct. doi:10.1016/j.ijsolstr.2016.02.005
88. Barbagallo G, Madeo A, Azehaf I et al. (2016) Bias extension test on an unbalanced woven composite reinforcement: experiments and modeling via a second gradient continuum approach. J Compos Mater, accepted 2016
89. Durville D (2010) Simulation of the mechanical behaviour of woven fabrics at the scale of fibers. Int J Mater Form 3(2):1241–1251
90. Gatouillat S, Bareggi A, Vidal-Salle E, Boisse P (2013) Meso modelling for composite preform shaping - simulation of the loss of cohesion of the woven fibre network. Compos Part A 54: 135–144
91. Boisse P, Gasser A, Hagege B, Billoet JL (2005) Analysis of the mechanical behaviour of woven fibrous material using virtual tests at the unit cell level, Int. J Mater Sci 40: 5955–5962

92. Boisse P (2007) Finite element analysis of composite forming. composites forming technologies, Woodhead publishing, 46–79
93. Badel P, Vidal-Salle E, Boisse P (2008) Large deformation analysis of fibrous materials using rate constitutive equations. Comput Struct 86:1164–1175
94. Charmetant A, Vidal-Salle E, Boisse P (2011) Hyperelastic modelling for mesoscopic analyses of composite reinforcements. Compos Sci Technol 71:1623–1631
95. de Bilbao E, Soulat D, Hivet G, Gasser A (2010) Experimental study of bending behaviour of reinforcements. Exp Mech 50(3): 333–351
96. Liang B, Hamila N, Peillon M, Boisse P (2014) Analysis of thermoplastic prepreg bending stiffness during manufacturing and of its influence on wrinkling simulations. Compos Part A 67:111–122
97. Syerko E, Comas-Cardona S, Binetruy C (2015) Models for shear properties/behavior of dry fibrous materials at various scales: a review. Int J Mater Form 8(1):1–23